

Geophysical Research Letters

RESEARCH LETTER

10.1029/2021GL094263

Key Points:

- The cause of rapid sea level drops observed during glaciations is unclear
- Ice saddles form abruptly even during gradual climate cooling
- A model of Laurentide ice sheet glaciation simulates rapid sea level drop from ice-dome mergers

Supporting Information:

Supporting Information may be found in the online version of this article.

Correspondence to:

W. Ji,
wwji@pku.edu.cn

Citation:

Ji, W., Robel, A., Tziperman, E., & Yang, J. (2021). Laurentide ice saddle mergers drive rapid sea level drops during glaciations. *Geophysical Research Letters*, 48, e2021GL094263. <https://doi.org/10.1029/2021GL094263>

Received 12 MAY 2021

Accepted 1 JUL 2021

Laurentide Ice Saddle Mergers Drive Rapid Sea Level Drops During Glaciations

Weiwen Ji^{1,2} , Alexander Robel³ , Eli Tziperman² , and Jun Yang¹ 

¹Department of Atmospheric and Oceanic Sciences, School of Physics, Peking University, Beijing, China, ²School of Earth and Atmospheric Sciences, Georgia Institute of Technology, Atlanta, GA, USA, ³Department of Earth and Planetary Sciences, School of Engineering and Applied Sciences, Harvard University, Cambridge, MA, USA

Abstract Recent glacial periods have included several periods of rapid sea level drop that are still not well understood. Here we show that rapid sea level drops can occur due to merger of two separate ice sheets without correspondingly rapid climate forcing. Using the Parallel Ice Sheet Model (PISM), we simulate glaciation of the Laurentide Ice Sheet (LIS) by gradually decreasing equilibrium-line altitude (ELA). Merger of the extended Keewatin sector of the Laurentide Ice Sheet with Labrador sector of the Laurentide Ice Sheet south of Hudson Bay causes a positive feedback between increasing surface elevation and increasing surface mass balance in the merger region, leading to fast ice sheet growth. The simulated saddle merger of LIS lowers sea level by 20 m in less than 20 kyr with periods of sea level fall exceeding 2 m/kyr, similar to those observed in paleo-sea level records.

Plain Language Summary Sea level dropped by about 120 m over a period of more than 80,000 years during the last ice age, though during brief intervals it has dropped by more than 20 m in less than 10,000 years. However, the cause of these rapid sea level drops is not known. Using a computer model of the flow of the North American Ice Sheet, we show that ice sheets grow quickly when separate ice sheets merge due to the increase of elevation and snowfall rate in the merger region. The simulated quick growth of ice sheets leads to a fast decrease in equivalent sea level similar to the past sea level records, as freshwater is sequestered on land in the form of an enlarged ice sheet. This study may provide a general explanation for rapid sea level falls in past ice ages.

1. Introduction

Proxy reconstructions of past ice volume and global mean sea level show that 100 kyr glacier-interglacial cycling has dominated global sea level variability over the last 0.8 Ma (Grant et al., 2014; Spratt & Lisiecki, 2016). While the mechanism of the late Pleistocene ice ages are still not completely understood, many climate feedbacks have been proposed to take part, including isostatic adjustment (Pollard, 1982), amplification by CO₂ variations (Gildor et al., 2002; Sigman et al., 2010; Toggweiler, 1999), rapid sea ice feedbacks that lead to atmospheric temperature changes and thus control the snow accumulation over the ice sheets (Gildor & Tziperman, 2000), and more. Shorter than orbital time scales of ice volume and sea level change are also found to be important components of Pleistocene climate, notably including millennial-scale periods of rapid sea level rise, such as Meltwater Pulse 1A (Bard et al., 1996; Fairbanks, 1989). Using a coarse model of ice sheet flow and evolution, Gregoire et al. (2012) simulated a separation of the Cordilleran Ice Sheet (CIS) and Laurentide Ice Sheet (LIS) causing a large meltwater pulse, consistent with the sea level jump associated with Meltwater Pulse 1A, and the separation of two ice domes composing the Laurentide Ice Sheet causing another smaller meltwater pulse. Similarly, Robel and Tsai (2018) found that a simple model of ice saddle separation accounting only for ice saddle geometry and a simple elevation-dependent surface mass balance can explain the occurrence, timing and amplitude of such deglacial meltwater pulses. However, some dynamical processes like ice streams are not included in such models, which play an important role in ice sheet reconstruction and deglaciation (De Angelis & Kleman, 2005, 2007; Robel & Tziperman, 2016; Stokes & Clark, 2001).

Though much attention has been paid to rapid sea level rise during deglaciation, sea level reconstructions reveal many periods of rapid sea level fall at rates approaching mean rates of sea level rise during deglaciation (Figure 1; m/kyr). The purpose of this study is to provide an explanation for such periods of rapid

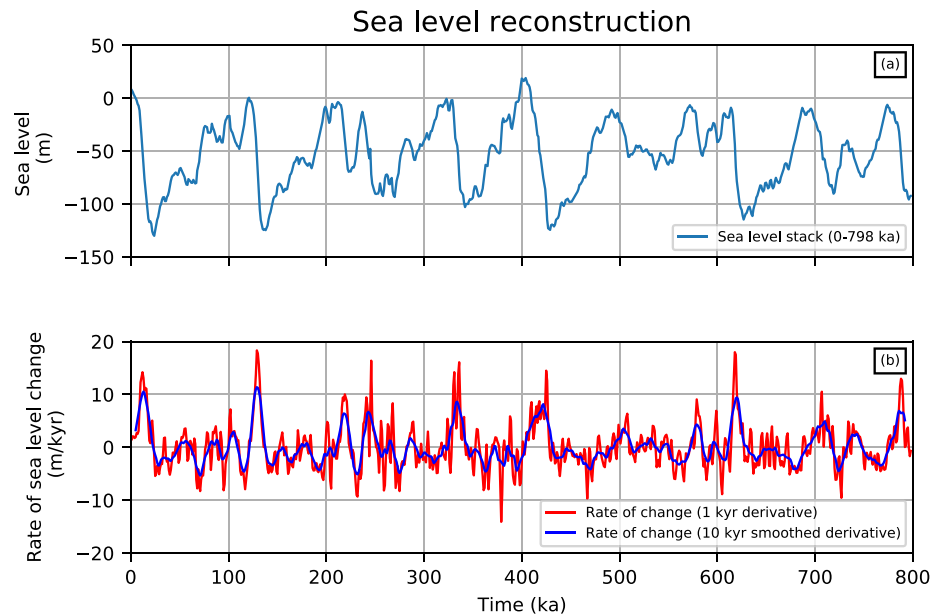


Figure 1. Reconstructed sea level changes. (a) The first principal component of the sea level from present to 798 kyr ago, and (b) the rate of sea level change (blue line shows the moving average of each 10 kyr). Data are from Spratt and Lisiecki (2016).

sea level fall, specifically the merging of distinct ice domes within the North American Ice Sheet Complex. Previous studies of rapid sea level fall events have mainly focused on measuring the timing and amplitude of these events (Chappell & Shackleton, 1986; Siddall et al., 2003; Waelbroeck et al., 2002). K. Cutler et al. (2003) realized that the generally flat terrain of interior North America allowed quick expansion of ice accumulation areas, and that low summer insolation value could lead to periods of rapid glaciation. The same study also posits the possibility that periods of enhanced advection of moisture into the continental interior may cause enhanced rates of glaciation and sea level fall. However, it should be noted that neither of these hypotheses are supported by calculations (model-based or otherwise) estimating the rates of sea level fall that could be generated by such physical processes.

In this study, we provide the first model-based explanation of periods of rapid sea level fall without an equally rapid period of climate change driving this fall. Specifically, we find that during the glaciation of the LIS, the “saddle merger” of two ice sheets will trigger fast ice sheet growth, leading to rapid sea level fall of 10–20 m over approximately 10 kyr, consistent with observed rapid sea level drop events. The proposed mechanism may be expected to occur during the glaciation of any multi-domed ice sheet. In Section 2, we describe the configuration of the numerical ice sheet model experiments. Then we analyze the saddle merger event simulated in this model and the resulting rapid sea level drop in Section 3. Summary and discussion are given in Section 4.

2. Model Setup

In order to capture realistic ice sheet processes including ice flow, ice sheet geometry, and their interaction with surface mass balance, we use the Parallel Ice Sheet Model (PISM) version 1.0 from the University of Alaska, Fairbanks (Bueler & Brown, 2009; the PISM authors, 2015). We use a hybrid stress balance scheme in PISM combining shallow ice and shallow shelf approximations to efficiently simulate both slow and fast flowing regions. The simulations are performed on a rectangular Cartesian coordinate system from a polar stereographic projection of the domain, containing the North America continent at 20 km horizontal resolution (451×351 grid cells). Though this is too coarse to represent grounding zones accurately, it is of sufficient resolution to simulate the geometry of land-based ice sheet margins, which are the focus of our analysis in this study. The bed topography is initialized at a modern state (National Geophysical Data

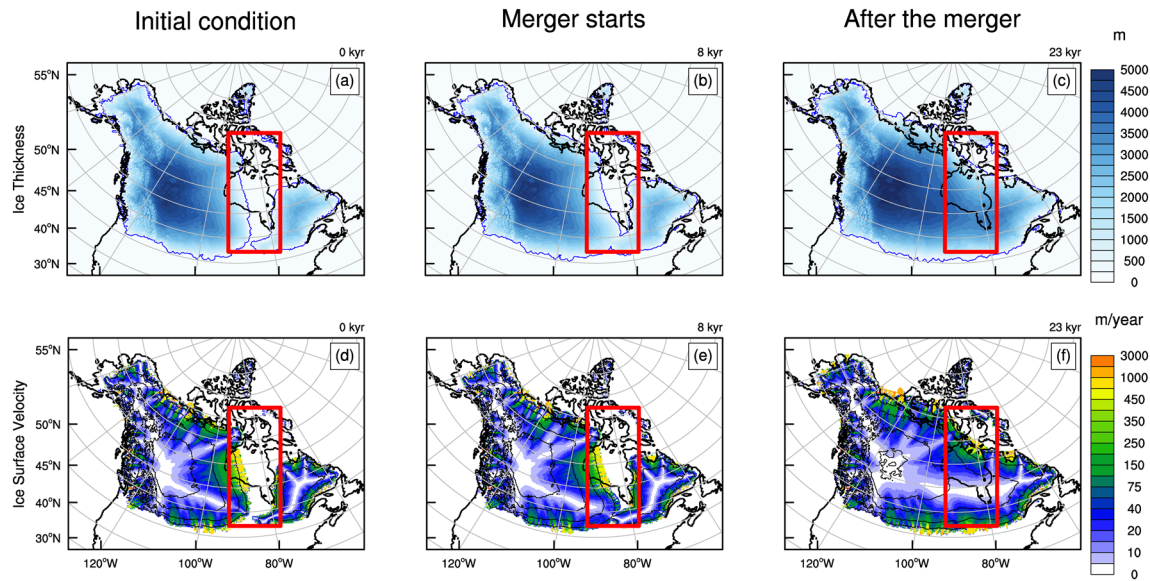


Figure 2. Snapshots of ice thickness and ice surface velocity. (a–c) The ice thickness and (d–f) the surface ice velocity. The first column is the initial condition for the simulation, the second column is at 8 kyr when the merger of the two ice sheets starts, and the third column is at 23 kyr after the merger of the two ice sheets. In each panel, the thick black lines indicate sea level, the blue lines show the ice sheet edges, and the red square shows the location where the saddle merger occurs. The thin black lines in the three lower panels are ice thickness contours with an interval of 1,000 m starting from 1,000 m.

Center, NESDIS, NOAA, U.S. Department of Commerce, 2001) and then allowed to adjust assuming an elastic lithosphere, relaxing to ice sheet loading (Lingle & Clark, 1985).

Due to the large uncertainties associated with climate forcing of ice sheets (at millennial time scales), the goal of this study is to determine the extent to which ice sheet geometry and dynamics alone can explain the rapid sea level drops in the absence of short-lived climate forcing (which may exist in some paleoclimate reconstructions, but be absent in others). Thus, we opt to prescribe the surface mass balance (SMB) on the ice sheet to vary linearly with ice sheet elevation and increasing toward the North. We set the surface mass balance anomaly (see Figure S2) at sea level to produce a steady-ice sheet extent that is, generally consistent with geological reconstructions of the ice sheet southern margins and volume at the Last Glacial Maximum (LGM, Roy & Peltier, 2018). The vertical SMB profile controls the growth and total steady state volume of the ice sheet. The SMB profile (see Figure S1) is negative at sea level and increases to a maximum value at 1 km height, and then declines exponentially toward high altitudes in line with observations of SMB variation with elevation for thick polar ice sheets (Boulton et al., 1984; P. M. Cutler et al., 2000). The till friction angle is specified based on a compilation of geological observations of sediment and bedrock properties over North America (see Figure S3, Gowan et al., 2019).

3. Results

We initiate a simulation of the Laurentide Ice Sheet from an ice-free modern bed topography with the equilibrium line at 700 m and run to a steady state (see Figure S8) as the initial condition for saddle merger event (Figures 2a and 2d). This initial ice sheet configuration includes two ice sheets separated by the Hudson Bay with ice streams discharging into Hudson Bay and at other land- and marine-terminating boundaries (Figure 2a). There are floating ice shelves on the west side of Hudson Bay which are fed by ice streams (Figure 2d). At the steady initial configuration, the Hudson Bay area separates ice sheets and has a negative mass balance without ice due to its low-elevation. The simulated ice sheet at this initially separated state has a small dome in Quebec, which is similar to previous reconstructions of pre-LGM ice sheets (Dyke et al., 2002; Gowan et al., 2021). As we use a prescribed surface mass balance profile with net accumulation at elevations over 700 m, the simulated ice sheet on the western side of Hudson Bay first grows on western high mountains and exhibits as an extended Keewatin sector of the Laurentide Ice Sheet expanding eastward with ice overgrown in Alaska, which is different from previous reconstructions with a smaller

ice dome restricted in Keewatin (Gowan et al., 2021). In reality, Alaska is warm, dry, and largely ice-free due to the influences of North American Ice Sheet Complex on atmospheric circulations (Löfverström & Liakka, 2016; Roe & Lindzen, 2001; Tulenko et al., 2020), which is not represented by our idealized climate forcing. Nonetheless, the dynamics we describe here are expected any time there are two nearby growing ice sheets, so this model configuration should be considered just one possible example.

We apply a gradual change in the prescribed surface mass balance profile by decreasing the ELA from 700 to 500 m linearly over 20 kyr to resemble a conservative estimate for ELA changes over obliquity cycles (Andrews et al., 1972; Pelto, 1992). This decreasing ELA leads to the growth and merger of the Keewatin sector and the Labrador sector of the Laurentide Ice sheets. Figure 2b shows the start of the merger between the two ice sheets (8 kyr). The merged region quickly increases in elevation due to the convergence of ice sheet flow, which in turn causes an increase in SMB (following the profile in Figure S1). The merger of separate ice sheets initiates the height-mass balance positive feedback between ice thickness and SMB (Oerlemans, 1981; Weertman, 1961), leading to the fast ice sheet growth. This merger process starts from the southern Hudson Bay and quickly covers the whole Hudson Bay. The ice surface velocities show that ice flow changes direction from primarily E-W (along the saddle long axis) to N-S (across the saddle short axis), causing an acceleration in ice sheet growth (Figure 2e). These changes are not qualitatively dependent on the speed of the ELA forcing (see Figures S4–S7).

After the merger (23 kyr), Hudson Bay is completely covered by ice including a greatly expanded marine terminus through which greater discharge balances the greater accumulation over the newly expanded ice sheet area (Figures 2c and 2f). The merged ice sheet has two peaks and displays a saddle shape along the merged area. The simulated ice sheet after the merger exhibits similar locations for ice domes as the ICE-7G reconstruction at the LGM (see Figure S9, Roy & Peltier, 2018).

Figure 3 shows the temporal evolution of the saddle merger event through diagnosis of the ice sheet mass balance components inside and outside of the merger region (occurring between the times marked by vertical dashed lines). The volume of the ice sheet has almost doubled with the decrease of ELA in 20 kyr (Figure 3a) and the snapshots in Figure 2 show that the increase of ice volume is mainly caused by ice growth in the merger region (See Figure S10 for difference in ice thickness). Meanwhile, the equivalent sea level dropped by more than 20 m and the maximum decline rate of 2 m/kyr occurs at about 18 kyr (Figure 3b).

The rate of sea level change can be decomposed into contribution due to SMB, ice discharge at the ice sheet margins, and basal mass balance (BMB) (Figure 3). The ice discharge and BMB are positive, causing sea level rise, while SMB and total mass balance contribution are negative, causing sea level fall. The basal heat flux in the model leads to the constant subglacial melting, thus small positive BMB in the unit of equivalent sea level. The SMB of the ice sheet in the beginning of our simulation continues to increase (shown as decreasing red line in Figure 3c) because the saddle merger event increases the ice sheet elevation in the merger region.

During the saddle merger event, the SMB of the merger region (indicated by the red square in Figure 2) dominates the total SMB change while the SMB of other areas changes little (Figure 3d). Near the end of the merger event, ice discharge in the merger region increases slightly due to the increased length of marine-terminating margin in Arctic Canada, compensating only slightly for the greatly increased SMB in the merger region. The dominance of SMB changes over discharge changes indicates the importance of the ice sheet merger, rather than potential marine ice dynamic flux changes (i.e., due to the marine ice sheet instability of the advancing ice sheet), in generating this rapid sea level fall. Since the saddle merger initiates above sea level (South of Hudson Bay), the rapid initial increase in SMB is not accompanied by an increase in ice discharge. By the end of the saddle merger event, the ice sheet margin has expanded into the Hudson Strait, producing enough ice discharge to balance the greatly increased SMB. Similar saddle mergers seen in reconstructions (e.g., Gowan et al., 2021) have a similar progression of rapidly increasing ice sheet elevation in the merger region, followed eventually by an increase in ice discharge through marine margins.

Figure 4 shows a schematic illustration of the mechanism of saddle merger: Isolated ice sheets expand relatively slowly at the edges as ELA is lowered (Figure 4a). However, when two separate ice sheets merge together, there is much less area of low-elevation melting margin, causing a significant increase in SMB (Figure 4b). Once the saddle merger occurs, ice flow reorients from being the direction of the proximate

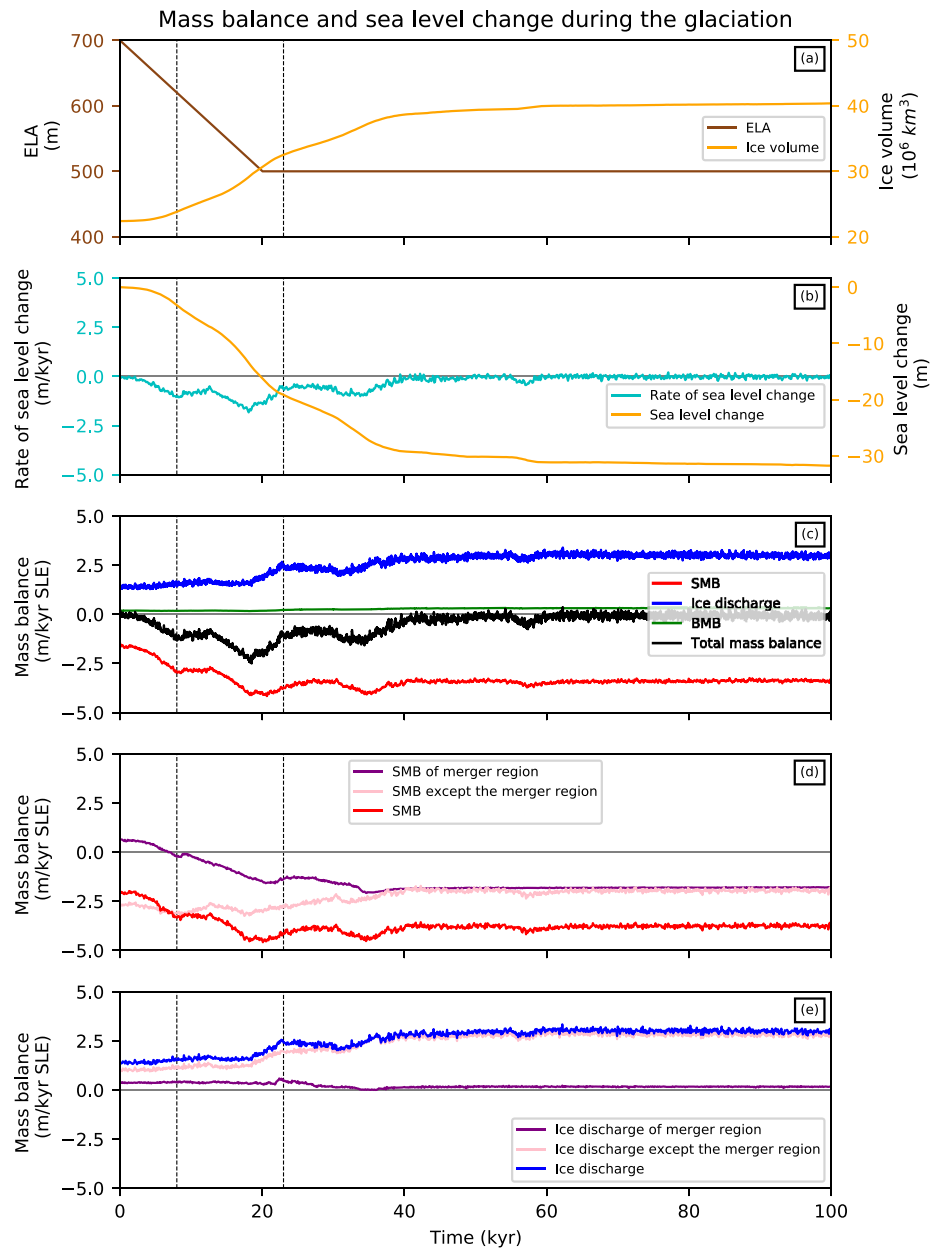


Figure 3. Ice sheet responses to the decrease of the equilibrium-line altitude (ELA) during one glaciation (the vertical dashed lines indicate the merger event). (a) The specified ELA (brown line) and the ice volume evolution (orange line); (b) the rate of sea level change (cyan line) and the change of sea level (orange line); (c) surface mass balance (SMB, red line), ice discharge to the ocean (blue line), basal mass balance (BMB, green line), and the total mass balance (black line); (d) SMB at the merger region (purple line), SMB outside the merger region (pink line), and the total SMB (red line; this line is the same as the red line in panel (c)); and (e) ice discharge to the ocean from the merger region (purple line), ice discharge outside the merger region (pink line), and the total discharge (blue line; this line is the same as the blue line in panel (c)). Both the mass balance and discharge are defined in the unit of sea level equivalent (SLE).

margins, to being across the newly formed ice saddle (toward the rapidly advancing Northern saddle margin, which is in Hudson Bay in our simulation). These perpendicular velocities accelerate the merging process by converging ice flow from the two ice domes. The saddle merger event combines small ice sheets into a larger one in a short time and triggers fast sea level fall. Different ice sheet reconstructions (e.g., Gowan et al., 2021; Stokes et al., 2012) include similar merger events occurring in various locations and times throughout the last glacial period. The goal of this study has been to model the dynamics of one such

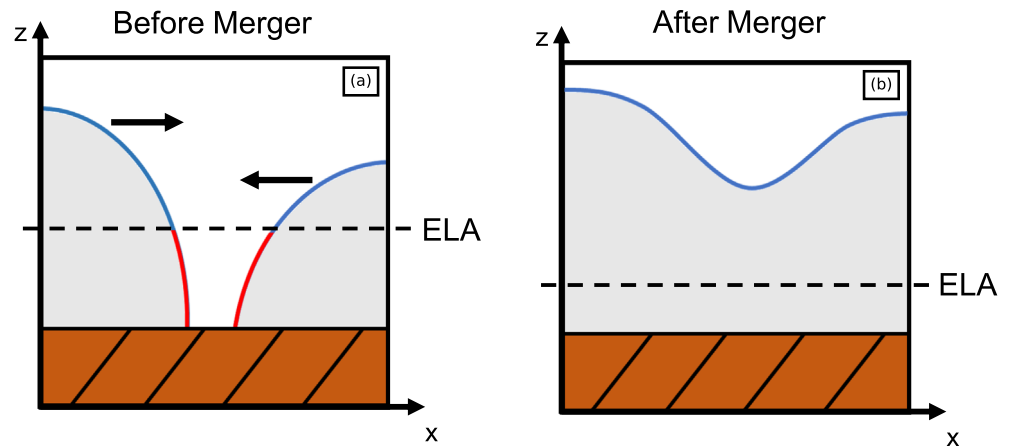


Figure 4. Schematic diagram illustrating the mechanism for the ice saddle merger. (a) Before the merger and (b) after the merger. Red lines show negative mass balance and blue lines show positive mass balance. The brown areas indicate the bottom topography. Vectors in (a) show the direction of ice flow. ELA, equilibrium-line altitude.

event, even if the specific dynamics of this event are not identical to reconstructions, which are themselves subject to considerable uncertainty from sparse observations and differences in the representation of physical processes in ice sheet models.

4. Summary and Discussion

The main finding of our work is that a saddle merger during the glaciation of the North American Ice Sheet Complex under a slowly and gradually decreasing ELA can cause sudden and rapid sea level fall, offering a potential explanation for some of the many periods of abrupt sea level fall during Northern Hemisphere glaciations (K. Cutler et al., 2003). Our simulations show that a saddle merger south of Hudson Bay leads to a sea level drop of more than 20 m in less than 20 kyr. This saddle merger event comes from the quick increase in ice sheet elevation when separate ice sheets merge, causing SMB to increase, resulting in fast ice sheet growth and sea level fall. The merger process triggers the positive height-mass balance feedback in the merger region, which follows the prescribed gradient as Figure S1 in this study.

Though constraining the extent of ice sheets prior to the LGM is complicated by the overprinting of glaciated landscapes (Hughes & Gibbard, 2018), there are a number of potential merger events in recent observationally constrained studies. Kleman et al. (2013) show in a simulation that merger events occur on North America and Europe at about 86.2 and 64 kyr ago. Batchelor et al. (2019) show many merger events of Northern Hemisphere ice sheets through the Quaternary. Gowan et al. (2021) (PaleoMIST 1.0) indicate two merger events (about 65 and 40 kyr ago) in Hudson Bay and one merger event (25 kyr ago) between Laurentide Ice Sheet and Cordilleran Ice Sheet.

Our simulated saddle merger event provides an interpretation for rapid sea level drops in paleo-sea level records. This saddle merger happens solely due to glaciological mechanisms even in the absence of rapid cooling in climate. One general implication from our simulations is that the glaciation of any multi-domed ice sheet, such as the North American Ice Sheet Complex or the Greenland Ice Sheet could potentially cause rapid sea level drops through saddle mergers. Saddle mergers may occur in a marine setting where increasing SMB over a rapidly growing saddle is accompanied by constant or decreasing ice flux at the marine margin. This is likely to occur where the bed is nearly flat or shallowing in the direction of ice flow (i.e., flat/retrograde beds). In such a scenario, rapid saddle merger and growth would occur in part due to increasing SMB and in part due to the marine ice sheet instability (Weertman, 1974).

Given the highly idealized nature of the climate forcing and the fact that we do not numerically constrain the model with observations of ice sheet extent or thickness, this study should be viewed as a proof of concept to show how saddle merger event produces rapid sea level drops, rather than a reconstruction of specific part of periods of sea level fall. The merger of ice sheets may respond differently in pace and

magnitude with a more realistic and evolving SMB. Growing ice sheets would induce a high pressure anti-cyclonic circulation and strengthen cold air and drying, therefore greatly influence the SMB pattern (Roe & Lindzen, 2001). However, the positive height-mass balance feedback which drives the merger event is expected to occur under a wide range of more realistic conditions. These merger events could happen during the glaciation of different ice sheets and also for the same ice sheet as it merges and separates repeatedly during glacial periods (such as Laurentide Ice Sheet, Batchelor et al., 2019).

This saddle merger mechanism is effectively the reverse of the saddle collapse mechanism discussed in previous model studies (Gregoire et al., 2012; Robel & Tsai, 2018), which demonstrates that mechanisms that have been invoked to explain rapid sea level rises could potentially explain rapid sea level falls when occurring in reverse. There are numerous rapid sea level fall intervals (i.e., over 20 m of sea level fall in less than 20 kyr) throughout the Pleistocene, which punctuate periods of otherwise steady glaciation. The saddle merger mechanism could potentially be used as a general explanation for such rapid sea level falls.

Data Availability Statement

Data sets for this research are included in these papers: Gowan et al. (2019), Roy and Peltier (2018), and Spratt and Lisiecki (2016). The simulation data can be downloaded from the Mendeley Data, <http://dx.doi.org/10.17632/gh7fgddr3w.1>.

Acknowledgments

W. Ji was partly supported by the China Scholarship Council during a visit to Harvard University. A. Robel was supported by NSF OPP Grant 1735715 in the Arctic Natural Sciences program during part of this work. E. Tziperman was supported by NSF Climate Dynamics program (joint NSF/NERC funding) grant AGS-1924538, and thanks the Weizmann Institute for its hospitality during parts of this work. J. Yang was supported by the National Natural Science Foundation of China (NSFC) under grant 42075046. The authors would like to acknowledge high-performance computing support from Cheyenne (<https://doi.org/10.5065/D6RX99HX>) provided by NCAR's Computational and Information Systems Laboratory, sponsored by the National Science Foundation. The computations in this paper were also run on the FASRC Cannon cluster supported by the FAS Division of Science Research Computing Group at Harvard University. We thank Joshua Cuzzone and Evan J. Gowan for providing thoughtful and constructive reviews on the manuscript.

References

- Andrews, J. T., Barry, R. G., Bradley, R. S., Miller, G. H., & Williams, L. D. (1972). Past and present glaciological responses to climate in eastern Baffin Island. *Quaternary Research*, 2(3), 303–314. [https://doi.org/10.1016/0033-5894\(72\)90050-6](https://doi.org/10.1016/0033-5894(72)90050-6)
- Bard, E., Hamelin, B., Arnold, M., Montaggioni, L., Cabioch, G., Faure, G., & Rougerie, F. (1996). Deglacial sea level record from Tahiti corals and the timing of global meltwater discharge. *Nature*, 382, 241–244. <https://doi.org/10.1038/382241a0>
- Batchelor, C. L., Margold, M., Krapp, M., Murton, D. K., Dalton, A. S., Gibbard, P. L., et al. (2019). The configuration of Northern Hemisphere ice sheets through the Quaternary. *Nature Communications*, 10(1), 1–10. <https://doi.org/10.1038/s41467-019-11601-2>
- Boulton, G., Smith, G., & Morland, L. (1984). The reconstruction of former ice sheets and their mass balance characteristics using a non-linearly viscous flow model. *Journal of Glaciology*, 30(105), 140–152. <https://doi.org/10.3189/s0022143000005876>
- Bueler, E., & Brown, J. (2009). Shallow shelf approximation as a “sliding law” in a thermodynamically coupled ice sheet model. *Journal of Geophysical Research*, 114(F3). <https://doi.org/10.1029/2008JF001179>
- Chappell, J., & Shackleton, N. (1986). Oxygen isotopes and sea level. *Nature*, 324(6093), 137–140. <https://doi.org/10.1038/324137a0>
- Cutler, K., Edwards, R., Taylor, F., Cheng, H., Adkins, J., Gallup, C., et al. (2003). Rapid sea-level fall and deep-ocean temperature change since the last interglacial period. *Earth and Planetary Science Letters*, 206(3–4), 253–271. [https://doi.org/10.1016/s0012-821x\(02\)01107-x](https://doi.org/10.1016/s0012-821x(02)01107-x)
- Cutler, P. M., MacAyeal, D. R., Mickelson, D. M., Parizek, B. R., & Colgan, P. M. (2000). A numerical investigation of ice-lobe–permafrost interaction around the southern Laurentide ice sheet. *Journal of Glaciology*, 46(153), 311–325. <https://doi.org/10.3189/172756500781832800>
- De Angelis, H., & Kleman, J. (2005). Palaeo-ice streams in the northern Keewatin sector of the Laurentide ice sheet. *Annals of Glaciology*, 42, 135–144. <https://doi.org/10.3189/172756405781812925>
- De Angelis, H., & Kleman, J. (2007). Palaeo-ice streams in the Foxe/Baffin sector of the Laurentide Ice Sheet. *Quaternary Science Reviews*, 26(9–10), 1313–1331. <https://doi.org/10.1016/j.quascirev.2007.02.010>
- Dyke, A., Andrews, J., Clark, P., England, J., Miller, G., Shaw, J., & Veillette, J. (2002). The Laurentide and Innuitian ice sheets during the Last Glacial Maximum. *Quaternary Science Reviews*, 21(1–3), 9–31. [https://doi.org/10.1016/s0277-3791\(01\)00095-6](https://doi.org/10.1016/s0277-3791(01)00095-6)
- Fairbanks, R. G. (1989). A 17,000 year glacio-eustatic sea level record: Influence of glacial melting rates on the Younger Dryas event and deep-ocean circulation. *Nature*, 342, 637–642. <https://doi.org/10.1038/342637a0>
- Gildor, H., & Tziperman, E. (2000). Sea ice as the glacial cycles climate switch: Role of seasonal and orbital forcing. *Paleoceanography*, 15, 605–615. <https://doi.org/10.1029/1999pa000461>
- Gildor, H., Tziperman, E., & Toggweiler, R. J. (2002). Sea ice switch mechanism and glacial-interglacial CO₂ variations. *Global Biogeochemical Cycles*, 16(3), 6–1–6–14. <https://doi.org/10.1029/2001GB001446>
- Gowan, E. J., Niu, L., Knorr, G., & Lohmann, G. (2019). Geology datasets in North America, Greenland and surrounding areas for use with ice sheet models. *Earth System Science Data*, 11(1), 375–391. <https://doi.org/10.5194/essd-11-375-2019>
- Gowan, E. J., Zhang, X., Khosravi, S., Rovere, A., Stocchi, P., Hughes, A. L., et al. (2021). A new global ice sheet reconstruction for the past 80 000 years. *Nature Communications*, 12(1), 1–9. <https://doi.org/10.1038/s41467-021-21469-w>
- Grant, K., Rohling, E., Ramsey, C. B., Cheng, H., Edwards, R., Florindo, F., et al. (2014). Sea-level variability over five glacial cycles. *Nature Communications*, 5(1), 1–9. <https://doi.org/10.1038/ncomms6076>
- Gregoire, L. J., Payne, A. J., & Valdes, P. J. (2012). Deglacial rapid sea level rises caused by ice-sheet saddle collapses. *Nature*, 487(7406), 219–222. <https://doi.org/10.1038/nature11257>
- Hughes, P. D., & Gibbard, P. L. (2018). Global glacier dynamics during 100 ka Pleistocene glacial cycles. *Quaternary Research*, 90(1), 222–243. <https://doi.org/10.1017/qua.2018.37>
- Kleman, J., Fastook, J., Ebert, K., Nilsson, J., & Caballero, R. (2013). Pre-LGM Northern Hemisphere ice sheet topography. *Climate of the Past*, 9(5), 2365–2378. <https://doi.org/10.5194/cp-9-2365-2013>
- Lingle, C. S., & Clark, J. A. (1985). A numerical model of interactions between a marine ice sheet and the solid earth: Application to a West Antarctic ice stream. *Journal of Geophysical Research: Oceans*, 90(C1), 1100–1114. <https://doi.org/10.1029/jc090ic01p01100>
- Löfverström, M., & Liakka, J. (2016). On the limited ice intrusion in Alaska at the LGM. *Geophysical Research Letters*, 43(20), 11–030. <https://doi.org/10.1002/2016gl071012>

- National Geophysical Data Center, NESDIS, NOAA, & U.S. Department of Commerce. (2001). *ETOPO2, global 2 arc-minute ocean depth and land elevation from the US National Geophysical Data Center (NGDC)*. Research Data Archive at the National Center for Atmospheric Research, Computational and Information Systems Laboratory. Retrieved from <https://doi.org/10.5065/D6668B75>
- Oerlemans, J. (1981). Some basic experiments with a vertically integrated ice sheet model. *Tellus*, 33, 1–11. <https://doi.org/10.3402/tellusa.v33i1.10690>
- Pelto, M. S. (1992). Equilibrium line altitude variations with latitude, today and during the Late Wisconsin. *Palaeogeography, Palaeoclimatology, Palaeoecology*, 95(1–2), 41–46. [https://doi.org/10.1016/0031-0182\(92\)90164-z](https://doi.org/10.1016/0031-0182(92)90164-z)
- Pollard, D. (1982). A simple ice sheet model yields realistic 100 kyr glacial cycles. *Nature*, 296, 334–338. <https://doi.org/10.1038/296334a0>
- Robel, A. A., & Tsai, V. C. (2018). A simple model for deglacial meltwater pulses. *Geophysical Research Letters*, 45(21), 11–742. <https://doi.org/10.1029/2018gl080884>
- Robel, A. A., & Tziperman, E. (2016). The role of ice stream dynamics in deglaciation. *Journal of Geophysical Research: Earth Surface*, 121, 1540–1554. <https://doi.org/10.1002/2016JF003937>
- Roe, G. H., & Lindzen, R. S. (2001). The mutual interaction between continental-scale ice sheets and atmospheric stationary waves. *Journal of Climate*, 14(7), 1450–1465. [https://doi.org/10.1175/1520-0442\(2001\)014<1450:tmibcs>2.0.co;2](https://doi.org/10.1175/1520-0442(2001)014<1450:tmibcs>2.0.co;2)
- Roy, K., & Peltier, W. (2018). Relative sea level in the Western Mediterranean basin: A regional test of the ICE-7G_NA (VM7) model and a constraint on late Holocene Antarctic deglaciation. *Quaternary Science Reviews*, 183, 76–87. <https://doi.org/10.1016/j.quascirev.2017.12.021>
- Siddall, M., Rohling, E. J., Almogi-Labin, A., Hemleben, C., Meischner, D., Schmelzer, I., & Smeed, D. (2003). Sea-level fluctuations during the last glacial cycle. *Nature*, 423(6942), 853–858. <https://doi.org/10.1038/nature01690>
- Sigman, D. M., Hain, M. P., & Haug, G. H. (2010). The polar ocean and glacial cycles in atmospheric CO₂ concentration. *Nature*, 466(7302), 47–55. <https://doi.org/10.1038/nature09149>
- Spratt, R. M., & Lisiecki, L. E. (2016). A Late Pleistocene sea level stack. *Climate of the Past*, 12(4), 1079–1092. <https://doi.org/10.5194/cp-12-1079-2016>
- Stokes, C. R., & Clark, C. D. (2001). Palaeo-ice streams. *Quaternary Science Reviews*, 20(13), 1437–1457. [https://doi.org/10.1016/S0277-3791\(01\)00003-8](https://doi.org/10.1016/S0277-3791(01)00003-8)
- Stokes, C. R., Tarasov, L., & Dyke, A. S. (2012). Dynamics of the North American Ice Sheet Complex during its inception and build-up to the Last Glacial Maximum. *Quaternary Science Reviews*, 50, 86–104. <https://doi.org/10.1016/j.quascirev.2012.07.009>
- the PISM authors. (2015). *PISM, a Parallel Ice Sheet Model*. Retrieved from <http://www.pism-docs.org>
- Toggweiler, J. R. (1999). Variation of atmospheric CO₂ by ventilation of the ocean's deepest water. *Paleoceanography*, 14, 572–588. <https://doi.org/10.1029/1999pa900033>
- Tulenko, J. P., Lofverstrom, M., & Briner, J. P. (2020). Ice sheet influence on atmospheric circulation explains the patterns of Pleistocene alpine glacier records in North America. *Earth and Planetary Science Letters*, 534, 116115. <https://doi.org/10.1016/j.epsl.2020.116115>
- Waelbroeck, C., Labeyrie, L., Michel, E., Duplessy, J. C., McManus, J., Lambeck, K., et al. (2002). Sea-level and deep water temperature changes derived from benthic foraminifera isotopic records. *Quaternary Science Reviews*, 21(1–3), 295–305. [https://doi.org/10.1016/S0277-3791\(01\)00101-9](https://doi.org/10.1016/S0277-3791(01)00101-9)
- Weertman, J. (1961). Stability of ice-age ice sheets. *Journal of Geophysical Research*, 66(11), 3783–3792. <https://doi.org/10.1029/jz066i011p03783>
- Weertman, J. (1974). Stability of the junction of an ice sheet and an ice shelf. *Journal of Glaciology*, 13(67), 3–11. <https://doi.org/10.3189/S0022143000023327>

References From the Supporting Information

- Annan, J., & Hargreaves, J. C. (2013). A new global reconstruction of temperature changes at the Last Glacial Maximum. *Climate of the Past*, 9(1), 367–376. <https://doi.org/10.5194/cp-9-367-2013>
- Bassis, J., & Ultee, L. (2019). A thin film viscoplastic theory for calving glaciers: Toward a bound on the calving rate of glaciers. *Journal of Geophysical Research: Earth Surface*, 124(8), 2036–2055. <https://doi.org/10.1029/2019JF005160>
- Gowan, E. J., Niu, L., Knorr, G., & Lohmann, G. (2019). Geology datasets in North America, Greenland and surrounding areas for use with ice sheet models. *Earth System Science Data*, 11(1), 375–391. <https://doi.org/10.5194/essd-11-375-2019>
- Tulaczyk, S., Kamb, W. B., & Engelhardt, H. F. (2000). Basal mechanics of Ice Stream B, west Antarctica: 2. Undrained plastic bed model. *Journal of Geophysical Research: Solid Earth*, 105(B1), 483–494. <https://doi.org/10.1029/1999JB900328>

Supporting Information for “Laurentide ice saddle mergers drive rapid sea level drops during glaciations”

Weiwen Ji^{1,3}, Alexander Robel², Eli Tziperman³, and Jun Yang¹

¹Department of Atmospheric and Oceanic Sciences, School of Physics, Peking University, Beijing 100871, China

²School of Earth and Atmospheric Sciences, Georgia Institute of Technology, Atlanta, Georgia, USA

³Department of Earth and Planetary Sciences and School of Engineering and Applied Sciences, Harvard University, Cambridge, MA, USA

Contents of this file

1. Text S1
2. Figures S1 to S10

Text S1.

In PISM, the rates of ice deformation and sliding are determined by driving stress, internal stress within the ice, and basal friction. We model the basal shear stress (τ_b) through plastic deformation in the sub-ice till (when the magnitude of the sliding velocity does not vanish, $\|\mathbf{v}\| > 0$ and τ_c is the yield stress), $\tau_b = -\tau_c \mathbf{v}/\|\mathbf{v}\|$, which is supported by laboratory measurements of till deformation (Tulaczyk et al., 2000). In locations where no sliding occurs, the basal shear stress is equal to the driving stress. We choose the Mohr-Coulomb model defining yield stress as

$$\tau_c = (\rho g H - p_w) \tan \phi. \quad (1)$$

Here ϕ is the till friction angle, H is the ice thickness, and p_w is the pore water pressure. We specified the till friction angle (range from 10 to 30 degrees) based on a compilation of geological observations of sediment and bedrock properties over North America (Gowan et al., 2019). The till friction angle in areas with small grain size sediments is set sufficiently low to permit sliding. The pore water pressure p_w is determined by the effective thickness of basal stored liquid water W as

$$p_w = 0.95 \rho g H \left(\frac{W}{W_0} \right), \quad (2)$$

where $W_0 = 2$ m is the maximum stored water thickness we set at the base of the ice sheet. We also choose the routing

model in PISM for subglacial hydrology that allows horizontal transport of excess water to ensure conservation of water in the subglacial layer. In reality, beds below sea level near the ocean are likely to be saturated and slippery, which we prescribe in the model by reducing the basal yield stress to its minimum value at grid points of grounding lines.

The initial SMB vertical profile has an equilibrium-line altitude (ELA) of 700 m. The maximum value of mass balance at 1 km is 7/9 m.w.e/yr and the minimum mass balance at high altitudes (about 6 km) is 1/9 m.w.e/yr.

We set the ice surface temperature in PISM to vary horizontally and with ice sheet elevation representing: 1) meridional sea level temperature variations in Last Glacial Maximum (LGM) (Annan & Hargreaves, 2013), and 2) vertical lapse rate using the value of -9.8 K/km equal to the dry adiabatic lapse rate, considering that the atmosphere above the ice sheet is relatively cold and dry.

Ice calving is a significant component of the mass loss of glaciers and we use a thickness-based calving criterion in our model experiments. This calving method permits the generation of ice shelves but removes any floating ice that is thinner than a threshold thickness. We set the threshold as 300 m since observations show that ice shelf calving fronts are generally not thinner than this value (Bassis & Ultee, 2019). Nonetheless, calving does not play a significant role in the dynamics we focus on in this study.

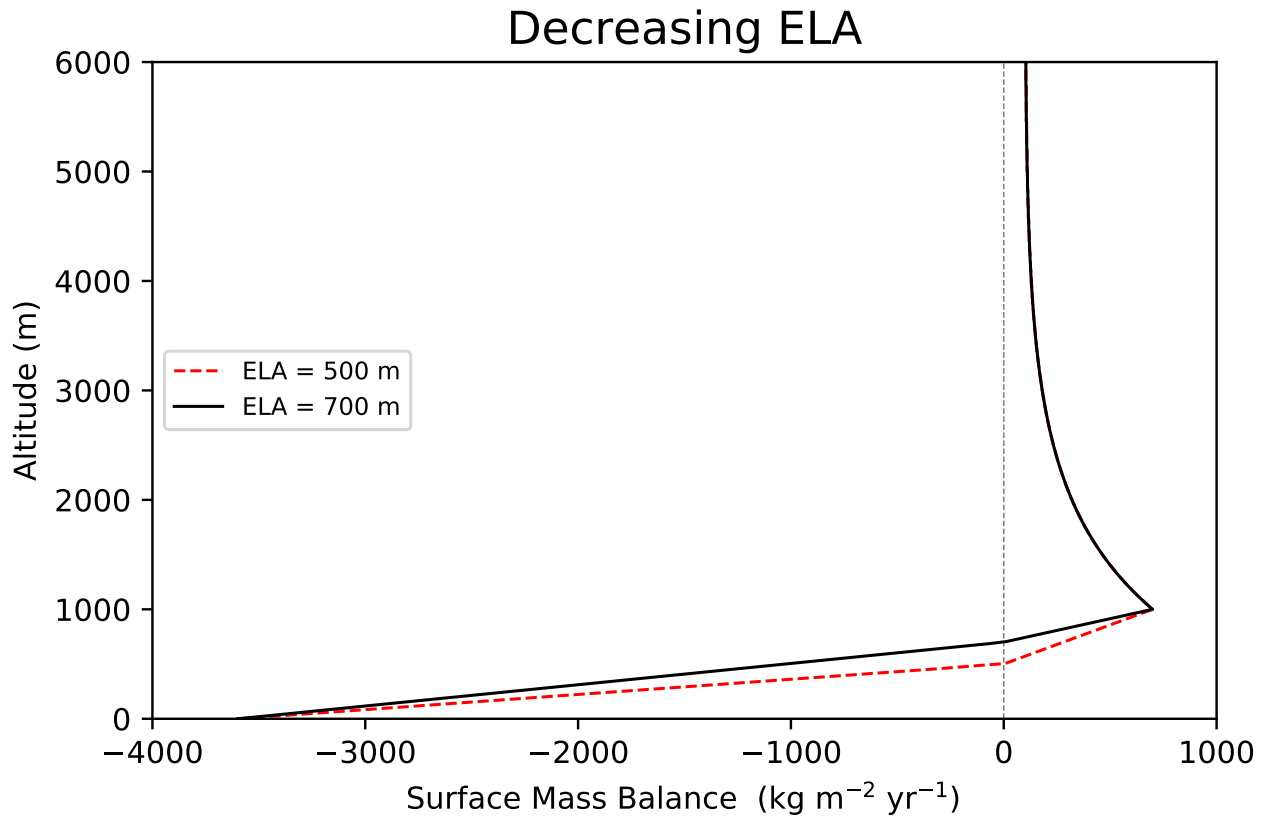


Figure S1: Vertical surface mass balance (SMB) profile decreasing equilibrium-line altitude (ELA). The black line shows the initial SMB profile (ELA equals 700 m) and the red dashed line shows that ELA decreases to 500 m. The maximum SMB at 1 km is $700 \text{ kg m}^{-2} \text{yr}^{-1}$ (7/9 m.w.e/yr) and the minimum SMB at 6 km is $100 \text{ kg m}^{-2} \text{yr}^{-1}$ (1/9 m.w.e/yr)

Surface Mass Balance Anomaly

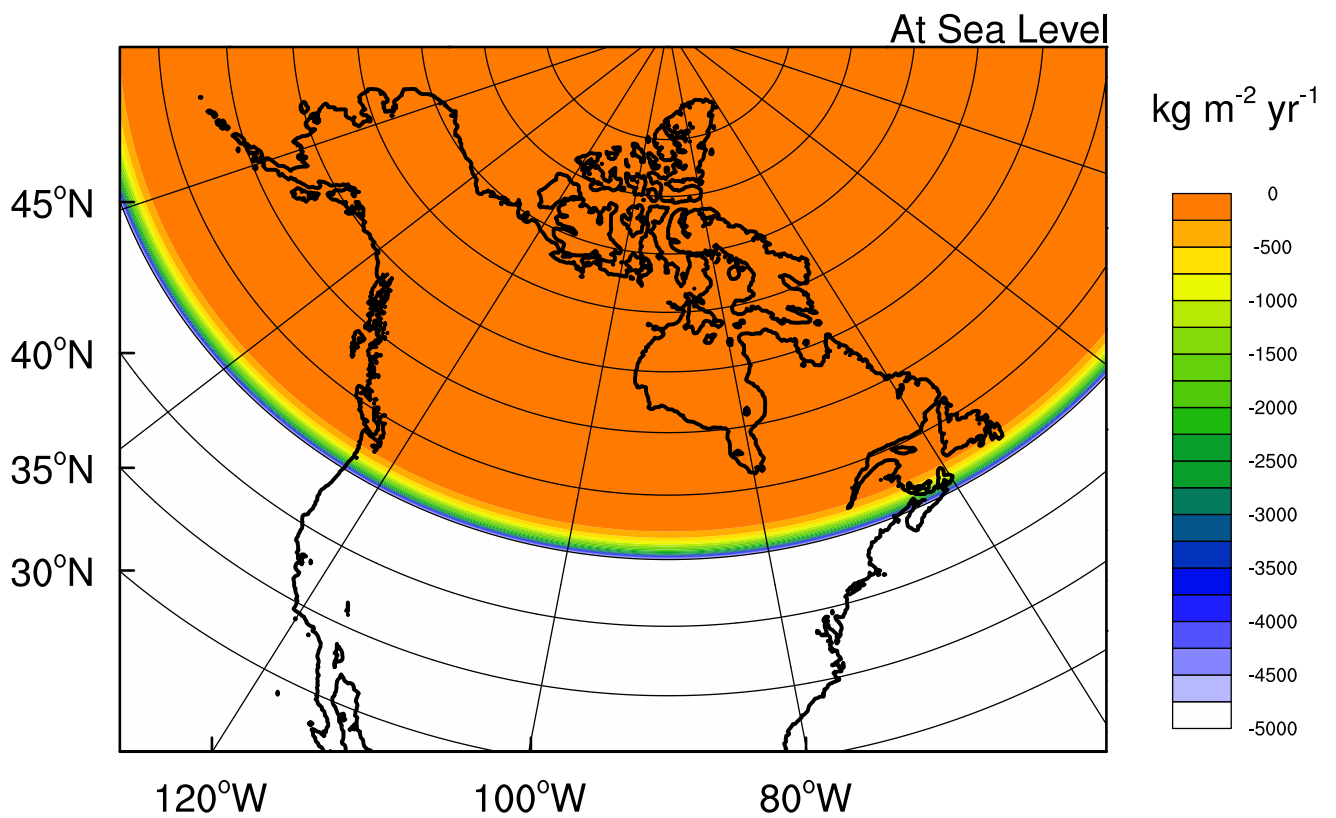


Figure S2: Surface mass balance (SMB) anomaly at sea level. This SMB anomaly constrains the ice sheet margin to 45 degrees North.

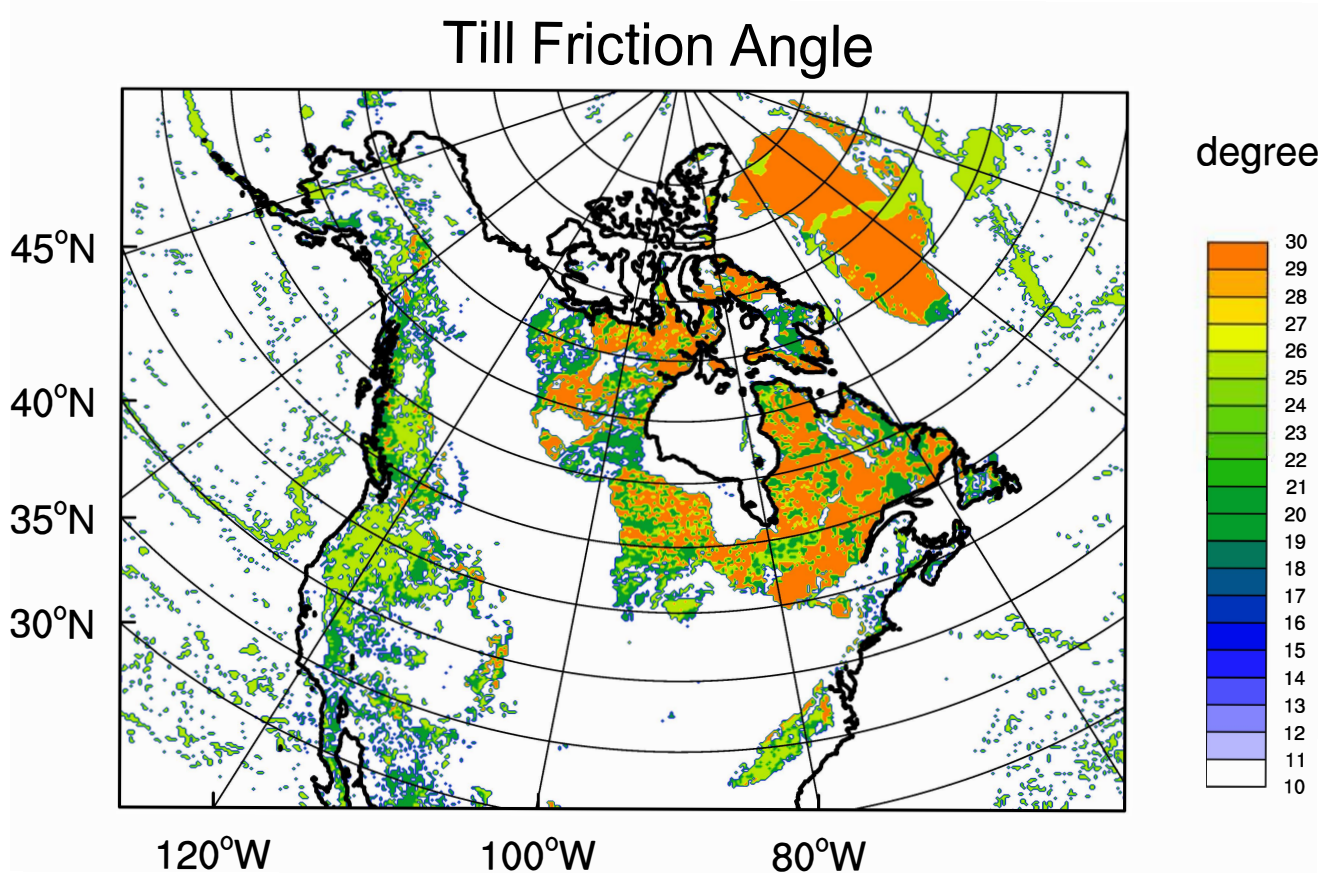


Figure S3: Specified till friction angle based on a compilation of geological observations of sediment and bedrock properties over North America (Gowan et al., 2019). The thick black line indicates sea level (without Greenland).

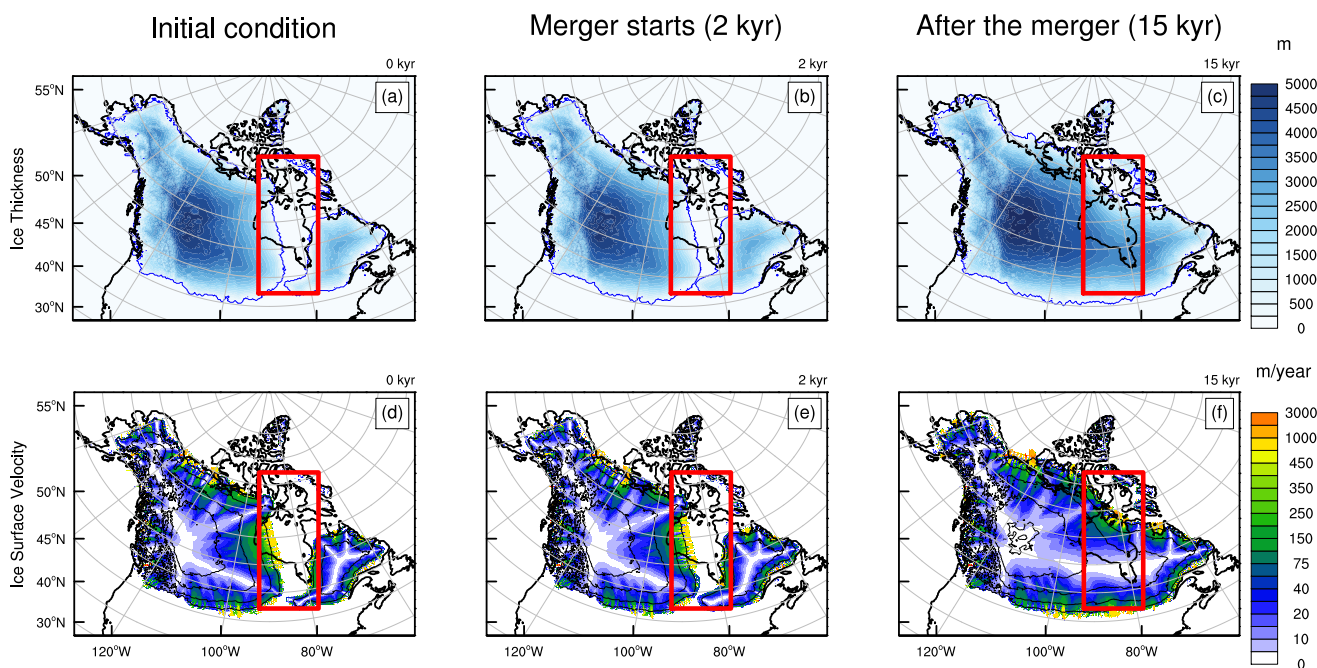


Figure S4: Snapshots of ice thickness and ice surface velocity (equilibrium-line altitude (ELA) **step changes** from 700 m to 500 m). (a–c) The ice thickness, and (d–f) the surface ice velocity. The first column is the initial condition for the simulation, the second column is at 2 kyr when the merger of the two ice sheets starts, and the third column is at 15 kyr after the merger of the two ice sheets. In each panel, the thick black lines indicate sea level, the blue lines show the ice sheet edges, and the red square shows the location where the saddle merger occurs. The thin black lines in the three lower panels are ice thickness contours with an interval of 1000 m starting from 1000 m.

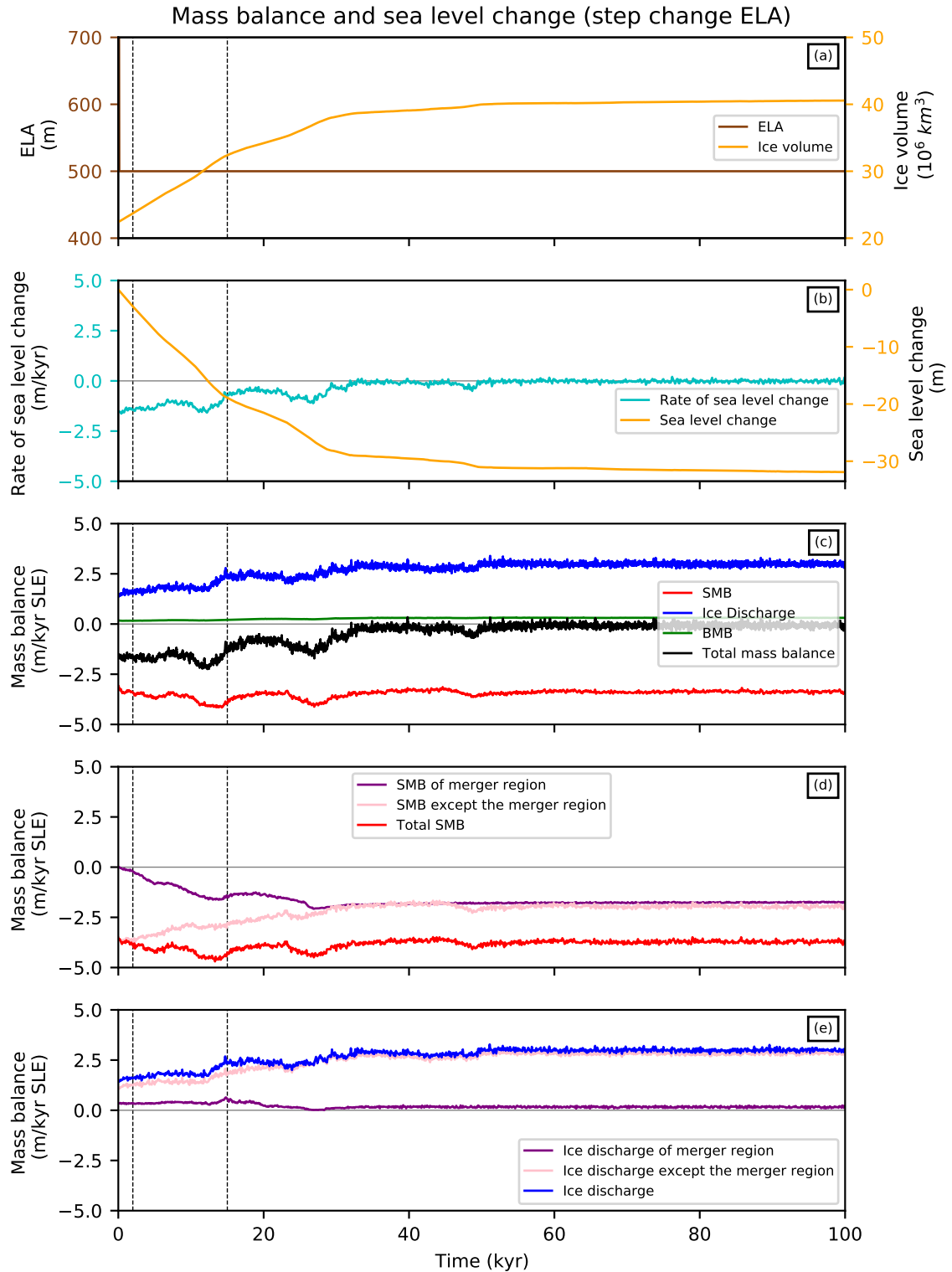


Figure S5: Ice sheet responses to the **step change** of the equilibrium-line altitude (ELA) during one glaciation (the vertical dashed lines indicate the merger event). (a): The specified ELA (brown line) and the ice volume evolution (orange line); (b): the rate of sea level change (cyan line) and the change of sea level (orange line); (c): surface mass balance (SMB, red line), ice discharge to the ocean (blue line), basal mass balance (BMB, green line), and the total mass balance (black line); (d): SMB at the merger region (purple line), SMB outside the merger region (pink line), and the total SMB (red line; this line is the same as the red line in panel (c)); and (e): ice discharge to the ocean from the merger region (purple line), ice discharge outside the merger region (pink line), and the total discharge (blue line; this line is the same as the blue line in panel (c)). Both the mass balance and discharge are defined in the unit of sea level equivalent (SLE).

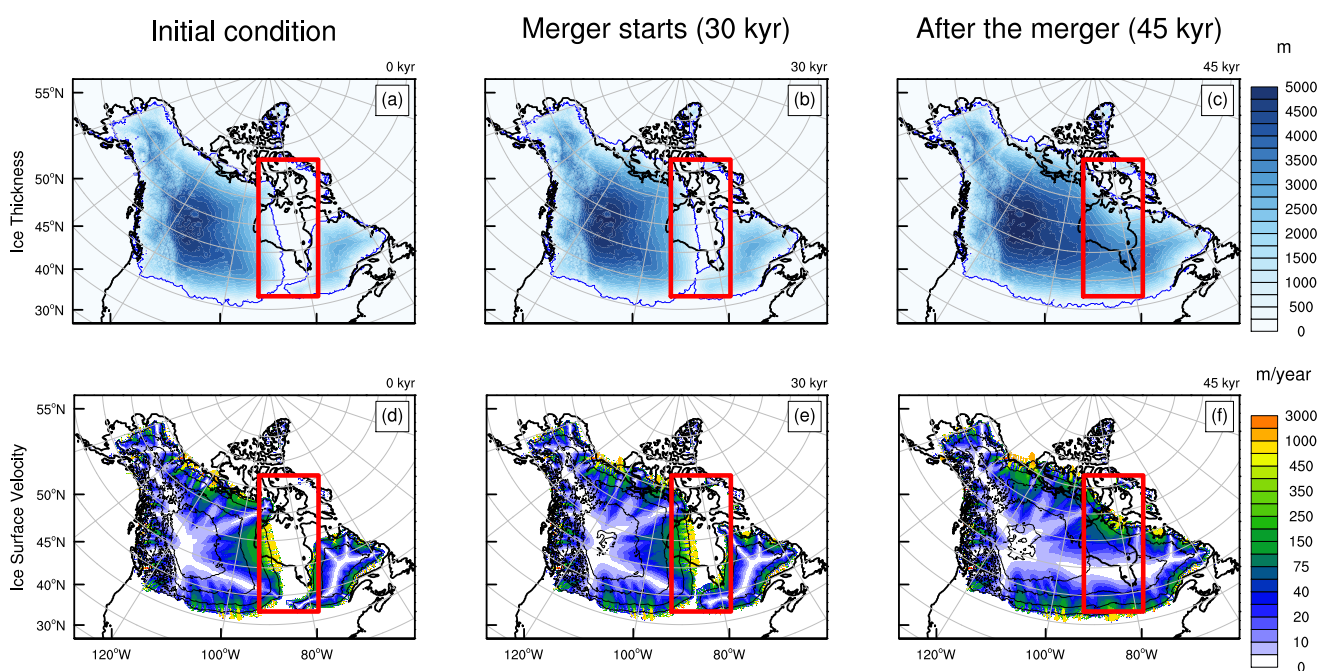


Figure S6: Snapshots of ice thickness and ice surface velocity (equilibrium-line altitude (ELA) linearly decreases from 700 m to 500 m in **100 kyr**). (a–c) The ice thickness, and (d–f) the surface ice velocity. The first column is the initial condition for the simulation, the second column is at 30 kyr when the merger of the two ice sheets starts, and the third column is at 45 kyr after the merger of the two ice sheets. In each panel, the thick black lines indicate sea level, the blue lines show the ice sheet edges, and the red square shows the location where the saddle merger occurs. The thin black lines in the three lower panels are ice thickness contours with an interval of 1000 m starting from 1000 m.

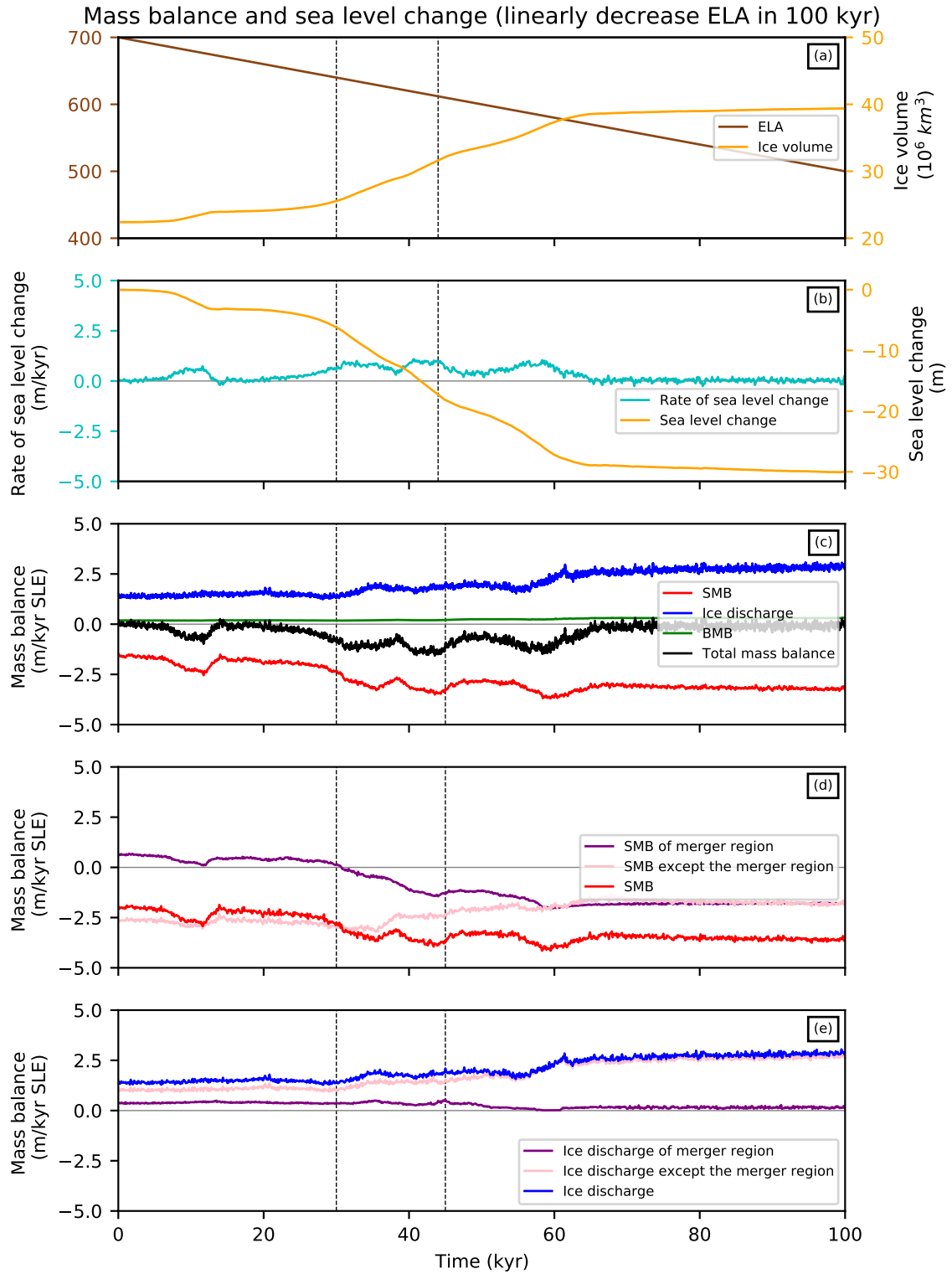


Figure S7: Ice sheet responses to the linear decrease of the equilibrium-line altitude (ELA) **over 100 kyr** (the vertical dashed lines indicate the merger event). (a): The specified ELA (brown line) and the ice volume evolution (orange line); (b): the rate of sea level change (cyan line) and the change of sea level (orange line); (c): surface mass balance (SMB, red line), ice discharge to the ocean (blue line), basal mass balance (BMB, green line), and the total mass balance (black line); (d): SMB at the merger region (purple line), SMB outside the merger region (pink line), and the total SMB (red line; this line is the same as the red line in panel (c)); and (e): ice discharge to the ocean from the merger region (purple line), ice discharge outside the merger region (pink line), and the total discharge (blue line; this line is the same as the blue line in panel (c)). Both the mass balance and discharge are defined in the unit of sea level equivalent (SLE).

Steady-state of the Initial Condition

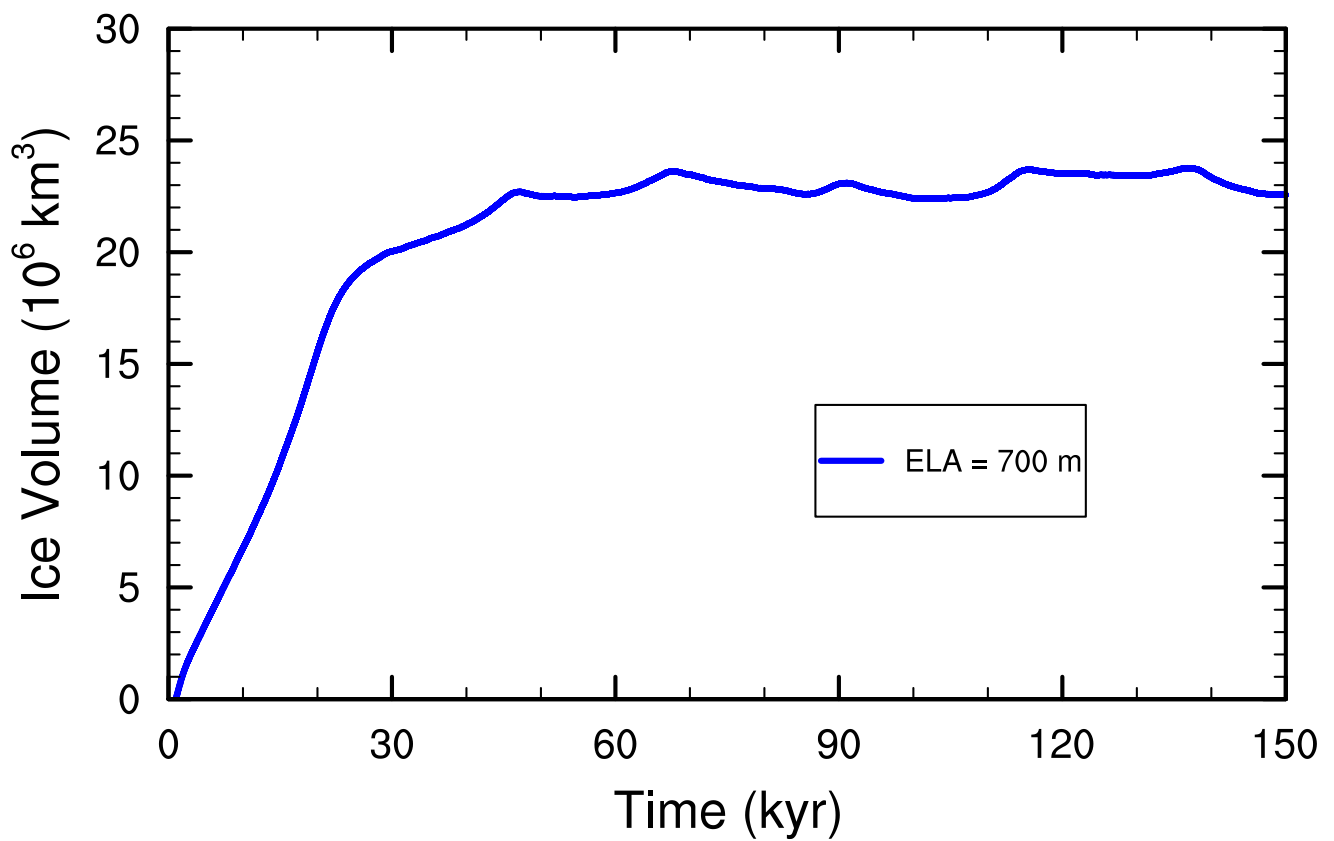


Figure S8: Time series of the modeled ice volume during the spinup. The initial prescribed surface mass balance (SMB) profile is shown as the black line in Figure S1 with an equilibrium-line altitude (ELA) of 700 m.

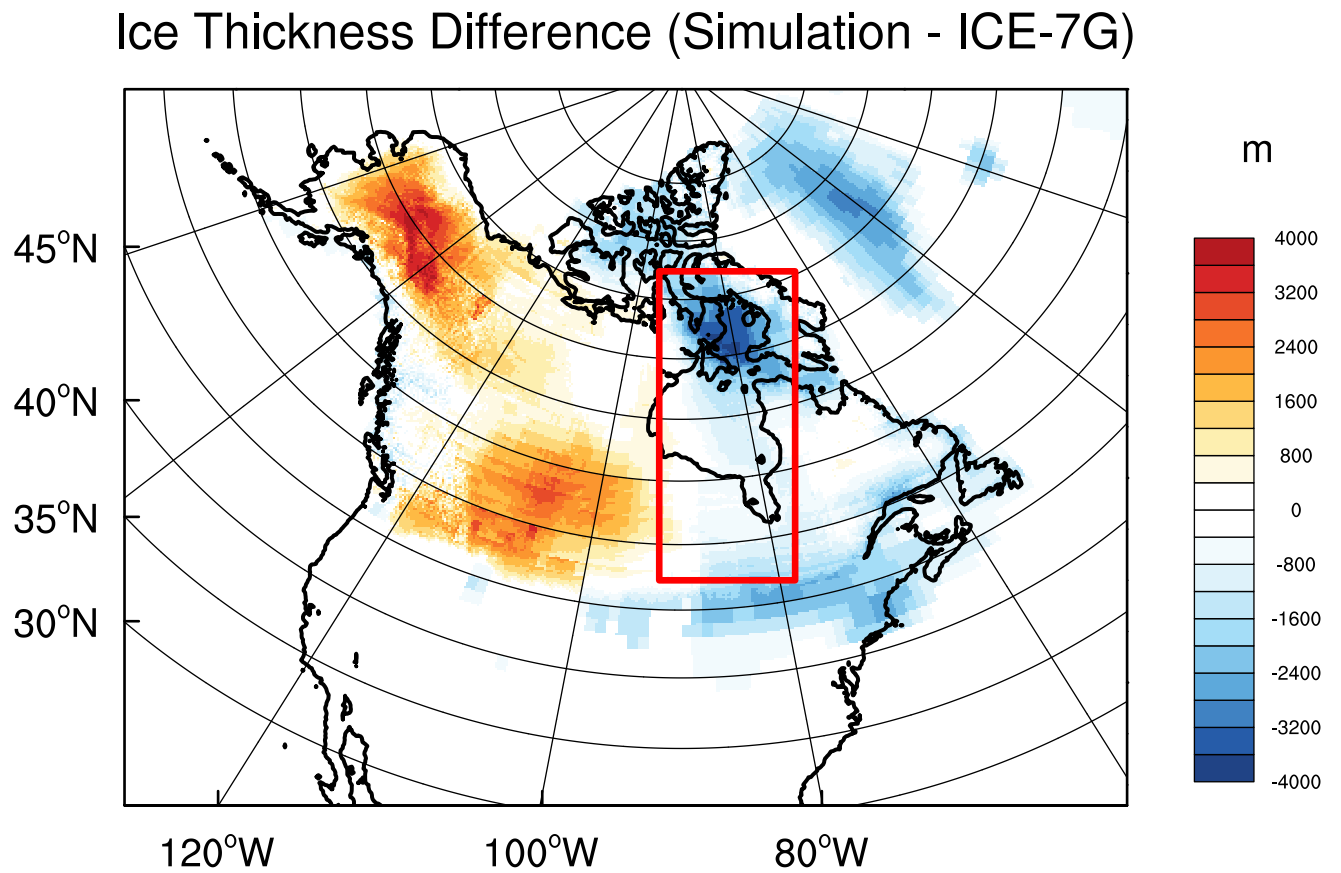


Figure S9: Ice thickness difference between simulation (after merger) and ICE-7G (26 ka) reconstructions. The red square shows the location where the saddle merger occurs.

Ice Thickness Difference (After Merger - Merger Starts)

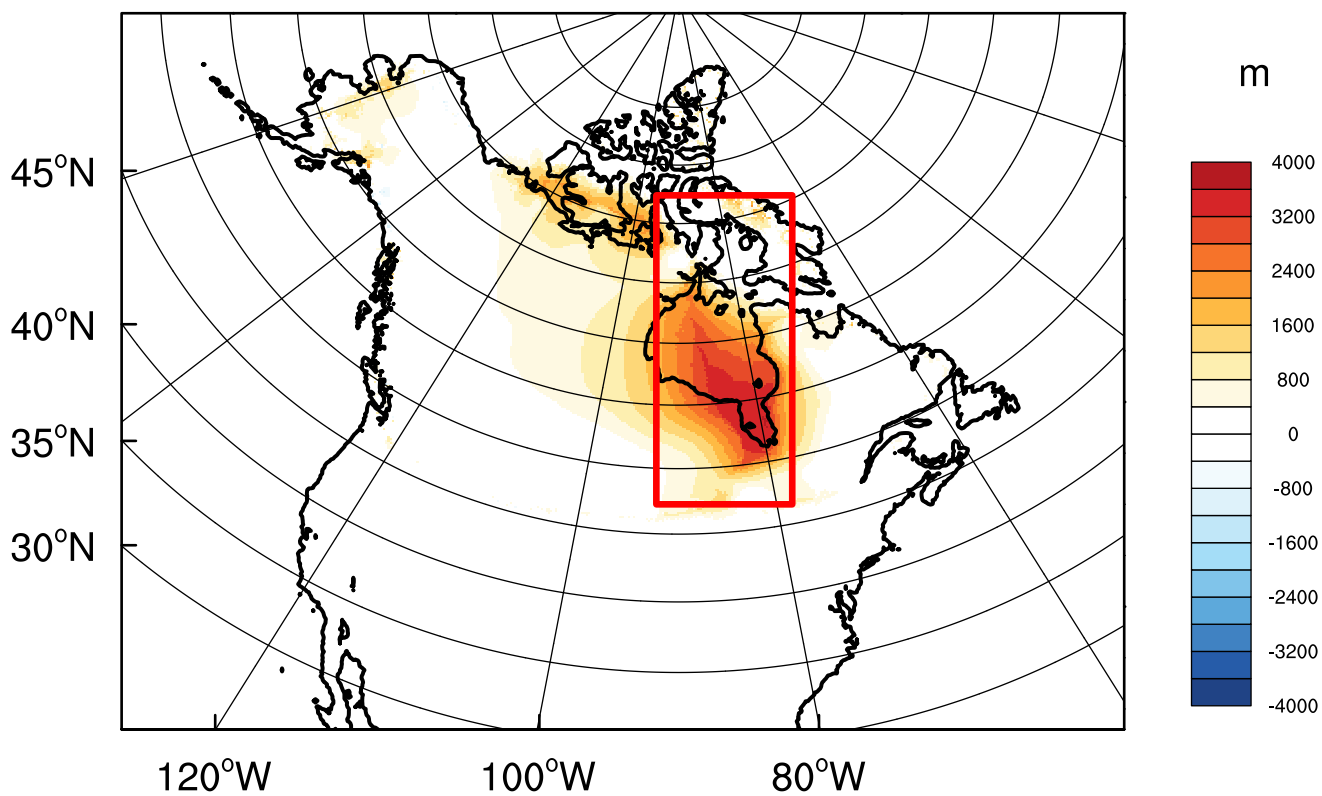


Figure S10: Ice thickness difference between Figure 3C (after merger) and 3B (merger starts). The red square shows the location where the saddle merger occurs.

References

- Annan, J., & Hargreaves, J. C. (2013). A new global reconstruction of temperature changes at the Last Glacial Maximum. *Climate of the Past*, *9*(1), 367–376.
- Bassis, J., & Ultee, L. (2019). A thin film viscoplastic theory for calving glaciers: Toward a bound on the calving rate of glaciers. *Journal of Geophysical Research: Earth Surface*, *124*(8), 2036–2055.
- Gowan, E., Niu, L., Knorr, G., & Lohmann, G. (2019). Geology datasets in north america, greenland and surrounding areas for use with ice sheet models. *Earth System Science Data*, *11*(1), 375–391.
- Tulaczyk, S., Kamb, W. B., & Engelhardt, H. F. (2000). Basal mechanics of ice stream b, west antarctica: 2. undrained plastic bed model. *Journal of Geophysical Research: Solid Earth*, *105*(B1), 483–494.